Acta Crystallographica Section B
Structural Science
ISSN 0108-7681

Transition from the incommensurately modulated structure to the lock-in phase in Co-åkermanite

Andreas K. Schaper,* Michael Schosnig, Ali Kutoglu, Werner Treutmann and Helmut Rager

Department of Geosciences and Materials Science Center, Philipps University Marburg, Hans-Meerwein-Strasse, D-35032 Marburg, Germany

Correspondence e-mail: schaper@mailer.uni-marburg.de

Received 3 October 2000
Accepted 25 April 2001

Dedicated to Professor Dr Hans-Georg von Schnering on the occasion of his 70th birthday.

The adaptation of the incommensurate structure modulation in $Ca_2CoSi_2O_7$ (dicalcium cobalt disilicate) single crystals to decreasing temperature has been examined using *in situ* high-resolution transmission electron microscopy and electron diffraction. The transition from the incommensurate to the commensurate lock-in phase of Co-åkermanite exhibits a pronounced hysteresis of a highly strained metastable state with a characteristic microdomain morphology. A network of domain walls surrounding single orientation domains develops out of the room-temperature tartan pattern, the domains increase in size and their alignment changes from crystallographic to random. At 100 K the phase transition becomes almost complete. In parallel, the evolution of the modulation structure can be described by a change from a loose arrangement of octagonal tilings into a close-packed configuration of overlapping octagons in the commensurate low-temperature lock-in phase. Thereby, the octagon represents the ordered distribution of low-coordinated Ca clusters within a nanodomain extending over 4 × 4 subunits, on average [Riester *et al.* (2000). *Z. Kristallogr.* **215**, 102–109]. The modulation wavevector was found to change from $\mathbf{q}_{1,2} = 0.295$ ($\mathbf{a}^* \pm \mathbf{b}^*$) at 300 K to $\mathbf{q}_{1,2} = 0.320$ ($\mathbf{a}^* \pm \mathbf{b}^*$) at 100 K.

1. Introduction

Melilite-type compounds have the general formula $X_2T^1T_2^2O_7$ with a large X cation, *e.g.* Na, Ca, Sr or Ba, and with small cations, such as Mg, Co, Fe, Al on the T^1 site and Al, Si, Ge on the T^2 site. The symmetry of the average melilite structure is tetragonal with space group $P\bar{4}2_1m$. Within the tetrahedral sheets two $[T^2O_4]$ tetrahedra are corner-linked to form $[T_2^2O_7]$ dimers, and these dimers are again linked through their corners to the surrounding four $[T^1O_4]$ tetrahedra. In the **c**-axis view of Fig. 1, the irregular pentagonal arrangements of the tetrahedra form large channels filled with the X cations which are located halfway between successive sheets along the **c** axis.

Numerous melilite compounds occur as solid solution minerals in natural rock assemblages. Moreover, special end-members of the melilite series have been synthesized because of their interesting structural features and potential applications as laser active materials (Hazenkamp *et al.*, 1995; Scott *et al.*, 1997).

The general reason for the formation of temperature-dependent modulation structures in melilites is the misfit between the intermediate X cation layer and the sheet-like tetrahedral framework (Seifert *et al.*, 1987; Armbruster *et al.*, 1990; Röthlisberger *et al.*, 1990). Direct evidence of this

behavior comes from structural studies of melilites with systematically varied chemistry (Röthlisberger *et al.*, 1990; Jiang *et al.*, 1998). Accomodation of the misfit strains within the lattice is provided by deformation of the tetrahedral layers *via* rotation about **c** of the T^2 tetrahedra within the $[T_2^2O_7]$ dimers, rotation parallel and perpendicular to the layer planes, and twisting of the T^1 tetrahedra (Van Heurck *et al.*, 1992; Tamura *et al.*, 1996). The rotational distortions are accompanied by considerable atomic displacements. The most prominent displacements are those of the O atoms bridging the T^2–T^2 and T^1–T^2 tetrahedra, which implicates even large distortions of the coordination polyhedra of the interlayer Ca atoms (Hagiya *et al.*, 1993; Yang *et al.*, 1997; McConnell, 1999; McConnell *et al.*, 2000; Riester *et al.*, 2000). According to recent interpretations the incommensurate modulation in melilites can be directly attributed to particular ordering schemes of low-coordinated calcium sites (Riester *et al.*, 2000).

$Ca_2CoSi_2O_7$ is known to show an incommensurately modulated superstructure at room temperature (*e.g.* Iishi *et al.*, 1990; Brown *et al.*, 1994; Tamura *et al.*, 1996; Riester & Böhm, 1997). The **a**-axis lattice parameter of the basic tetragonal unit cell of 7.842 Å, according to Hagiya *et al.* (1993) (Kimata, 1983, reported 7.826 Å), is associated with an average wavelength of $\lambda \simeq 19$ Å of the two-dimensional displacive modulation. The incommensurate room-temperature phase transforms into a non-modulated normal phase at ~490 K (Hagiya *et al.*, 1993). Below 160 K the occurrance of a stable lock-in phase has been reported (Riester & Böhm, 1997). Recent X-ray single-crystal experiments suggest that the superstructure of this phase is nearly commensurate (Riester *et al.*, 2000). Detailed electron diffraction and microscopic observations of the modulation structure in Co-åkermanite have been lacking until now.

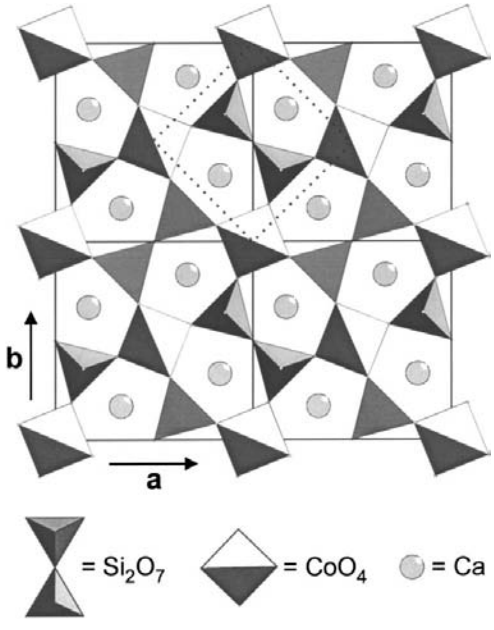

Figure 1
Supercell of the average structure of $Ca_2CoSi_2O_7$ melilite projected on the (001) plane. The dotted line represents a subunit comprising one Si_2O_7 dimer.

In a related paper we have discussed the temperature and composition dependence of the normal-to-incommensurate phase transition of Ca,Sr-åkermanites as deduced from electron diffraction investigations (Schosnig *et al.*, 2000). The present paper is a transmission electron microscope (TEM) and electron diffraction (TED) study of Co-åkermanite and focuses on the structural changes during the first-order phase transition if one goes from the incommensurately modulated room-temperature phase to the low-temperature lock-in phase.

2. Experimental

Powders of high-grade $CaCO_3$, CoO and SiO_2 were weighted in stoichiometric proportions, mixed in an agate mortar, pressed into pellets and calcined in an alumina crucible at 1273 K. The calcined powder was mixed again in an agate mortar, pressed into a hard metal tube of 8 mm diameter and loaded into a high-pressure piston-cylinder apparatus at 1 kbar. $Ca_2CoSi_2O_7$ melts congruently at 1591 K. Rods of 25–40 mm length were sintered in air at 1453 K for 10 h. For the preparation of single crystals we used a double ellipsoid mirror furnace with halogene lamps (maximum 450 W) as the heating source. The nutrient rods were counter-rotated with 30 r.p.m. Usually, a crystal growth rate of 1.0 mm h^{-1} was applied. Further details as to the mirror furnace device and the crystal growth technique are given in Geray (1990).

For transmission electron microsopy, single crystals were cut into thin sections and glued into 3 mm diameter Ti disks. The crystals were aligned with their **c** axis normal to the disk plane. The samples were mechanically thinned down to 50 μm

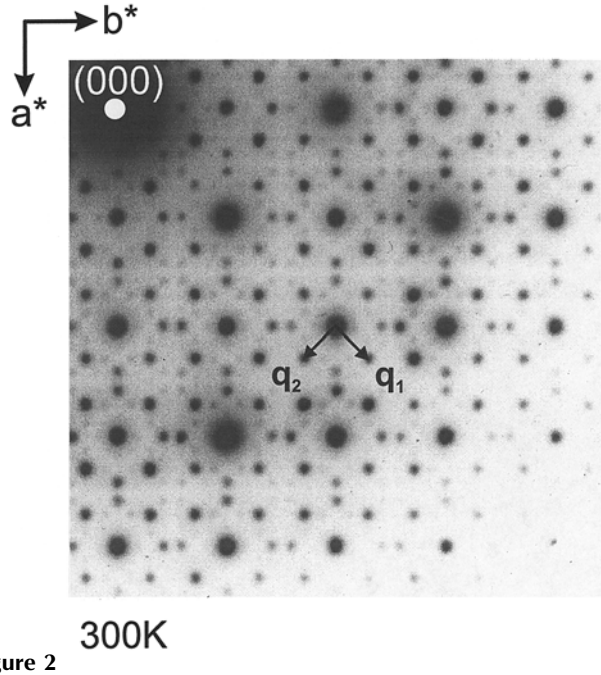

Figure 2
Typical [001] electron diffraction pattern of incommensurate Co-åkermanite at 300 K revealing up to second-order satellite reflections. The modulation wavevectors $\mathbf{q}_1 = \alpha\,(\mathbf{a}^* + \mathbf{b}^*)$ and $\mathbf{q}_2 = \alpha\,(\mathbf{a}^* - \mathbf{b}^*)$ are indicated.

and subsequently Ar-ion milled in a Technoorg-Linda IV3 H/L ion milling machine under low angles (< 4°) until perforation occurred. The TEM experiments were performed using a JEM 3010 electron microscope operated at 300 kV. For the investigations at low temperatures a Gatan 613-50DH double tilt cooling holder was used.

3. Results

Fig. 2 shows a typical (*hk*0) electron diffraction pattern of the Co-åkermanite structure at room temperature. The basic tetragonal reflections are surrounded by satellite reflections which belong to two equivalent sets of modulation waves with the wavevectors $\mathbf{q}_1 = \alpha(\mathbf{a}^* + \mathbf{b}^*)$ and $\mathbf{q}_2 = \alpha\,(\mathbf{a}^* - \mathbf{b}^*)$ along the reciprocal lattice directions [110] and [$\bar{1}$10]. Satellites up to second order are detected. From this and other diffraction diagrams an average value of $\alpha = 0.295$ has been determined. Thus, the structure is, in two dimensions, incommensurately modulated with a room-temperature modulation wavelength of $\lambda = 18.8$ Å.

Due to the intertwining of the two modulation waves, a tartan-patterned superstructure is revealed within the thicker parts of the Co-åkermanite TEM sample, such as that shown in the electron micrograph of Fig. 3 at medium magnification. The appearance of the tartan pattern is synonymous with the existence of nanometer-sized domains as they were observed in Zn,Ge-melilites by Van Heurck *et al.* (1992).

Upon closer inspection of the modulation structure by high-resolution imaging, in Fig. 4 details of the incommensurate atomic arrangements are discerned. Along the modulation directions [110] and [$\bar{1}$10] atomic arrays are detected which alternatingly show variations in density and brightness of the dots. For the most intense lines two major sequences of approximately 16.5 and 22 Å are deduced from the micrograph. These spacings correspond very closely to three and four times the dimension of a subunit outlined in Fig. 1. In Co-åkermanite the subunit contains one [Si_2O_7] dimer and two Ca atoms, with the corners being occupied by Co atoms. Obviously, the nanodomains in the incommensurately modulated structure are formed by a particular aggregation of the Co-framed subunits. As illustrated by the overlay drawing in Fig. 4 and discussed later in this paper, a possible tiling for the modulation pattern is provided by octagonal cell arrangements. The alignment of the cells varies between almost periodic and non-periodic from one to another sample area.

The structural mechanisms accompanied with the phase transition process are of particular interest. Fig. 5 shows the evolution of the incommensurate phase towards the commensurate lock-in phase after keeping the sample, during the first cooling cycle, at a temperature of 100 K for 100–150 min. In Fig. 5(*a*) the crystal area shown is intersperced with a network of intersecting domain boundaries running almost parallel to the basic crystallographic **a** and **b** axes. The size of the majority of the microdomains is in the magnitude of 10 nm; a few domains as large as 100 nm are also visible. Prolonged cooling leads to the structure image of Fig. 5(*b*) showing a random network of domain boundaries with considerably increased domain sizes up to > 200 nm. Some remains of the crystallographic alignment of single boundary segments can be detected in the bottom of the micrograph.

Fig. 6 shows a many-beam bright-field image taken during the progressing phase transition in the time interval given by Figs. 5(*a*) and (*b*), while the temperature was held constant at 100 K. Within this snapshot several interesting observations can be made. One striking feature is the pattern of modulation fringes oriented parallel to [110] and [$\bar{1}$10] showing a slight waviness and a shift when crossing the domain boundaries.

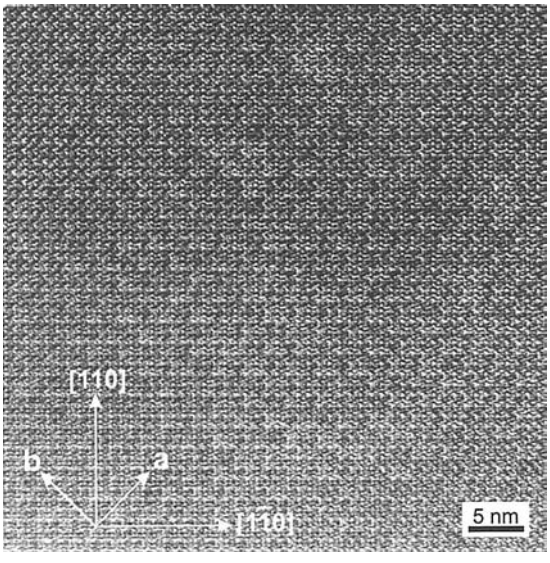

Figure 3
Transmission electron micrograph at medium resolution revealing a tartan-like pattern formed by intersecting of the two modulation waves along [110] and [$\bar{1}$10].

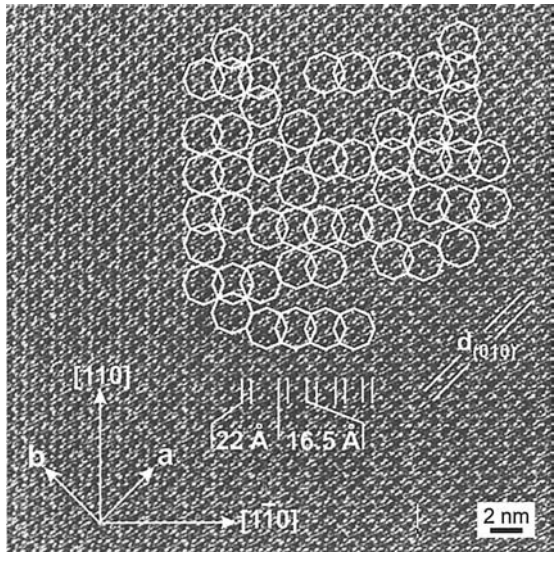

Figure 4
High-resolution electron micrograph of the modulation structure at 300 K with a possible octagonal tiling representing the modulation nanodomains overlaid. Variation of the modulation sequence is provided by a partial overlapping of the octagons..

The magnitude of the shift, deduced from areas such as those arrowed in the micrograph, varies between $2/3\pi$ and π, and has thus no clear antiphase character. Furthermore, the fringe spacing itself is determined to 13.4 Å, on average, which is much smaller than the modulation wavelength reported above. The simple explanation is that the fringes revealed are parallel moiré patterns formed by the two sets of strong first-order satellites at the positions 0.295 ($\mathbf{a}^* \pm \mathbf{b}^*$) and 0.705 ($\mathbf{a}^* \pm \mathbf{b}^*$). It is to be suggested that the intensity diffracted into these spots contains even contributions from mutual double diffraction. Hence, even though we do not see the modulation structure directly, the corresponding moiré patterns are a clear expression of it. Therefore, in Fig. 6 it can be further distinguished between microdomains with one (D_1) or the other (D_{21}, D_{22}) of the two modulation directions dominating. Microdomains where both intersecting modulation waves equally occur are not very frequent. At some places, the micrograph in Fig. 6 exhibits, in addition, the (100) lattice planes which the moiré pattern forms an angle of 45° with.

During cooling it has proved difficult to obtain a definite diffraction pattern. Starting at ~140 K, the intensities and amplitudes of the diffraction spots have become extremely unstable. Stable conditions were obtained only after lowering the temperature down to 100 K and after the application of repeated cooling cycles. This behavior clearly indicates that the crystal undergoes a strong phase transitional process. The final situation, under the experimental conditions applied, is represented by Fig. 7. In contrast to the 300 K diffraction pattern, the satellite reflections take positions on a square grid with mesh size of approximately 1/3 of the basic reciprocal lattice vectors. From a number of diffraction patterns we determined an average value $\alpha = 0.320$. This is in close agreement with the results of the X-ray structure determination of the lock-in phase by Riester *et al.* (2000) and yields an average modulation wavelength $\lambda = 17.3$ Å. The slight deviation from the exactly commensurate case can be verified looking at the TED pattern along the ⟨110⟩ directions under glancing incidence.

Fig. 8 is a high-resolution electron microscope image of the 100 K Co-åkermanite structure corresponding to the diffraction pattern of Fig. 7. The microdomain boundary network almost completely disappeared, which unambiguously indicates relaxation of the accumulated internal stresses. In comparison with the irregular arrangement of nanodomains in the incommensurate structure at 300 K comprising modulation sequences of three and four subunit dimensions, at 100 K a highly regular arrangement of the nanodomains is observed

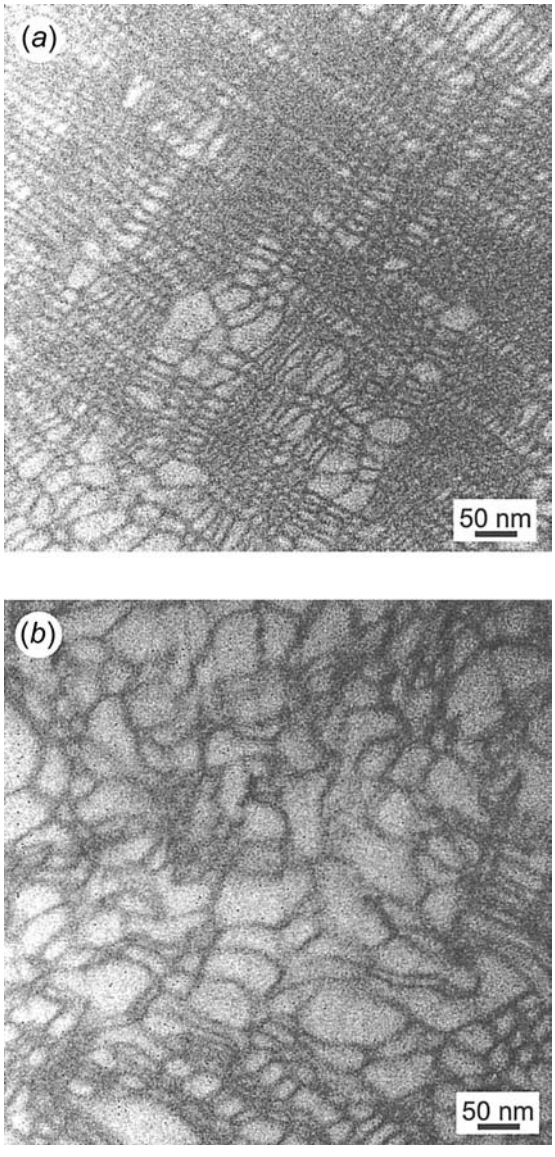

Figure 5
Evolution of a microdomain morphology in juvenile Co-åkermanite in the metastable transition region between the incommensurate phase and the commensurate lock-in phase after holding the sample for (*a*) 100 min and (*b*) 150 min at 100 K.

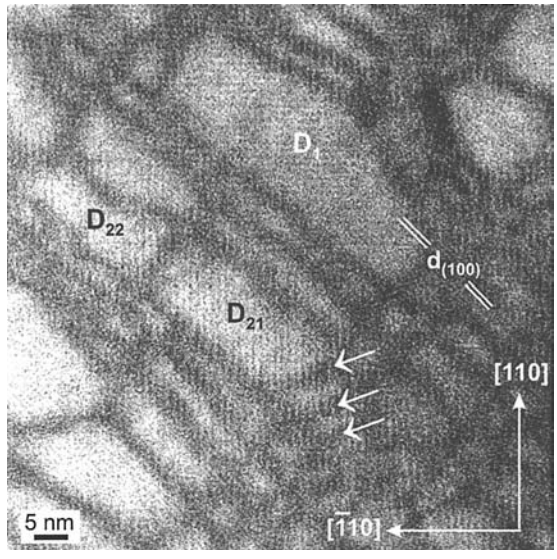

Figure 6
Many-beam bright-field image of an intermediate situation between Figs. 5(*a*) and (*b*) displaying single orientation microdomains with the modulation vector directed along [110] in domain D_1, and along [$\bar{1}$10] in domains D_{21} and D_{22}. The structure modulation is revealed by parallel moiré fringes, which show a characteristic phase shift crossing the domain walls (see arrows). The (100) lattice spacing is marked.

with a uniform modulation sequence of about three subunits. The modulation period derived from TED is confirmed by the transmission electron micrograph in Fig. 8.

4. Discussion

The observations presented in this paper show that the structure of the two-dimensional incommensurate modulation of Co-åkermanite at room temperature is characterized by a non-periodic arrangement of nanodomains. In the case where both modulation waves are intersecting and of similar amplitude, the nanodomains form a tartan-like pattern as known from the studies of $Ca_2ZnGe_2O_7$ by Van Heurck *et al.* (1992). If one follows the considerations of these authors each nanodomain represents a set of well matched structural subunits with a distinguished tilt pattern of the constituent polyhedral entities, the tilt pattern changes alternatingly from one to the other nanodomain. In the high-resolution image of Fig. 3, a proper fit for the arrangement of the nanodomains within the modulated structure has been found using a net of octagonal tilings similar to the one proposed by Van Heurck *et al.* (1992) and by Riester *et al.* (2000). Although the outlined net is only one possibility of different complex arrangements, it principially confirms the phenomenon of clustering of structural units as a route to accomodate internal stresses. Also proven is a partial overlapping of a number of neighboring octagons which automatically yields varying modulation sequences, the average value being close to the TED modulation wavelength λ = 18.8 Å corresponding to the intermediate spacing of three- and fourfold subunit combinations. This is analogous to the display of intermediate spacings observed in mixed-layer structures (Drits & Tchoubar, 1990) and in $Ca_2ZnGe_2O_7$ melilites (Van Heurck *et al.*, 1992).

Approaching the phase transitional region at low temperature, after prolonged cooling time microscopic imaging reveals a dense network of some 10 nm-sized domains surrounded by domain walls. Usually, the microdomains are single orientational modulation domains. While the structure is still in the incommensurate state, separation of the two modulation waves into adjacent microdomains seems to be energetically the more favorable situation.

When the network appears, the microdomain walls are crystallographically well aligned along the *a* and *b* axes. With progressing phase transition, the domain structure becomes more and more disturbed and the crystallographic alignment destroyed, so that a widely random network of domain walls develops. Along with these changes the microdomains grow considerably in size. It is suggested that at this stage of the phase transitional process parts of the incommensurately modulated domains have already been transformed into the stable low-temperature lock-in phase. Therefore, the domain walls may be even called discommensurations (Janssen & Janner, 1987; Amelinckx & Van Dyck, 1993). The growth of the domains, at this stage of the transition, is synonymous with the growth of the distance between discommensurations whereby the wavevector reaches the commensurate value over an entire part of the crystal. In the past, similar processes were observed during charge density wave (CDW) phase transitions of certain transition-metal dichalcogenide layer crystals (Chen *et al.*, 1982).

The *in situ* diffraction experiments confirm that the transition from the incommensurately modulated room-temperature phase into the lock-in phase does not occur

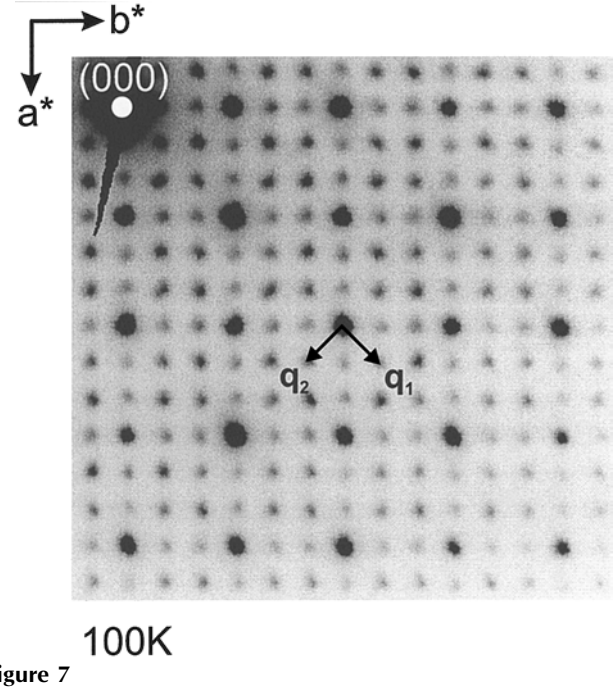

Figure 7
Typical [001] electron diffraction pattern of Co-åkermanite at 100 K after a prolonged equilibrium time. The wavevectors $\mathbf{q}_1$ and $\mathbf{q}_2$ indicate almost commensurate modulation.

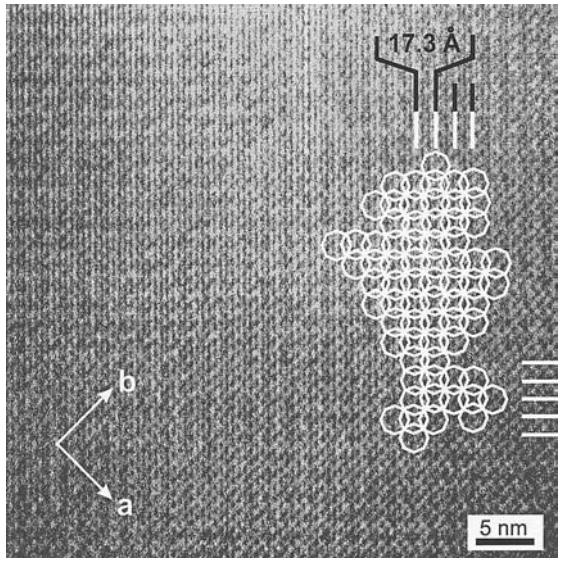

Figure 8
High-resolution electron micrograph of the low-temperature lock-in phase. A modulation wavelength around 17 Å is well established by complete overlap of the octagonal tiling.

spontaneously, but is time- and temperature-dependent over a rather large temperature interval. Repeated heating/cooling regimes are indicative of remarkable hysteresis effects within the temperature range $155 \leq T_c \leq 270$ K. Significant changes in the TED patterns are observed starting at a temperature of $\sim$140 K. Finally, after equilibration at 100 K, the commensurately modulated low-temperature superstructure is observed. The not exact commensurate data are in fair agreement with those from X-ray experiments (Riester *et al.*, 2000).

It is now widely accepted that the distortion of the Ca polyhedra and the accompanying reduction of the Ca coordination from eight- to sixfold are the predominant features in the evolution of the incommensurate modulation in melilites (Hagiya *et al.*, 1993; McConnell, 1999; McConnell *et al.*, 2000; Riester *et al.*, 2000). There are indications that the low-coordinated Ca sites form octagonal ordering patterns around the Co tetrahedra. It has been further suggested (Riester *et al.*, 2000), and our investigations confirm this view, that in the incommensurate phase the octagonal clusters are more or less statistically distributed with only partial overlap of the octagons. During transformation from the incommensurate phase into the stable lock-in phase, the concentration of low-coordinated Ca increases leading to a denser packing up to complete overlap of the octagonal ordering formations (Riester *et al.*, 2000). Hence, the lock-in phase appears to be stabilized by an ordered distribution of clusters of low-coordinated calcium. On the basis of these model calculations the present observations can be satisfactorily interpreted. Microscopic studies at especially high resolution are in progress to reveal the exact atomic configurations within the commensurate phase with even higher precision.

Funding by the Deutsche Forschungsgemeinschaft within the grant Ra554/9-1,2 is gratefully acknowledged.

References

Amelinckx, S. & Van Dyck, D. (1993). *Electron Diffraction Techniques*, edited by J. M. Cowley, Vol. 2, pp. 309–372. Oxford University Press.

Armbruster, T., Röthlisberger, F. & Seifert, F. (1990). *Am. Mineral.* **75**, 847–858.

Brown, N. E., Ross, C. R. & Webb, H. S. L. (1994). *Phys. Chem. Miner.* **21**, 469–480.

Chen, C. H., Gibson, J. M. & Fleming, R. M. (1982). *Phys. Rev. B*, **26**, 184–205.

Drits, V. A. & Tchoubar, C. (1990). *X-ray Diffraction by Disordered Lamellar Structures.* p. 371. Berlin: Springer.

Geray, R. (1990). Ph.D. Thesis. University of Marburg, Germany.

Hagiya, K., Ohmasa, M. & Iishi, K. (1993). *Acta Cryst.* B**49**, 172–179.

Hazenkamp, M. F., Oetliker, U., Güdel, H. U., Kesper, U. & Reinen, D. (1995). *Chem. Phys. Lett.* **233**, 466–470.

Iishi, K., Fujino, K. & Furukawa, Y. (1990). *Phys. Chem. Miner.* **17**, 467–471.

Janssen, T. & Janner, A. (1987). *Adv. Phys.* **36**, 519–624.

Jiang, J. C., Schosnig, M., Schaper, A. K., Ganster, K., Rager, H. & Tóth, L. (1998). *Phys. Chem. Miner.* **26**, 128–134.

Kimata, M. (1983). *Neues Jahrb. Mineral. Abh.* **146**, 221–241.

McConnell, J. D. C. (1999). *Z. Kristallogr.* **214**, 457–464.

McConnell, J. D. C., McCammon, C. A., Angel, R. J. & Seifert, F. (2000). *Z. Kristallogr.* **215**, 669–677.

Riester, M. & Böhm, H. (1997). *Z. Kristallogr.* **212**, 506–509.

Riester, M., Böhm, H. & Petricek, V. (2000). *Z. Kristallogr.* **215**, 102–109.

Röthlisberger, F., Seifert, F. & Czank, M. (1990). *Eur. J. Mineral.* **2**, 585–594.

Schosnig, M., Schaper, A. K, Kutoglu, A., Treutmann, W. & Rager, H. (2000). *Z. Kristallogr.* **215**, 495–498.

Scott, M. A., Han, T. P. J., Gallagher, H. G. & Henderson, B. (1997). *J. Lumin.* **72–74**, 260–262.

Seifert, F., Czank, M., Simmons, B. & Schmahl, W. (1987). *Phys. Chem. Miner.* **14**, 26–35.

Tamura, T., Yoshiasa, A., Iishi, K., Takeno, S., Maeda, H., Emura, S. & Koto, K. (1996). *Phys. Chem. Miner.* **23**, 81–88.

Van Heurck, C., Van Tendeloo, G. & Amelinckx, S. (1992). *Phys. Chem. Miner.* **18**, 441–452.

Yang, H., Hazen, R. M., Downs, R. T. & Finger, L. W. (1997). *Phys. Chem. Miner.* **24**, 510–519.